The Journal of Immunology

RESEARCH ARTICLE | APRIL 15 2022

Mettl14-Mediated m6A Modification Is Essential for Germinal Center B Cell Response FREE

Hengjun Huang; ... et. al

J Immunol (2022) 208 (8): 1924–1936.
https://doi.org/10.4049/jimmunol.2101071

Mettl14-Mediated m6A Modification Is Essential for Germinal Center B Cell Response

Hengjun Huang,* Gaopu Zhang,* Gui-Xin Ruan,* Yuxing Li,* Wenjing Chen,* Jia Zou,† Rui Zhang,* Jing Wang,* Sheng-Jian Ji,* Shengli Xu,‡,§ and Xijun Ou*

The germinal center (GC) response is essential for generating memory B and long-lived Ab-secreting plasma cells during the T cell–dependent immune response. In the GC, signals via the BCR and CD40 collaboratively promote the proliferation and positive selection of GC B cells expressing BCRs with high affinities for specific Ags. Although a complex gene transcriptional regulatory network is known to control the GC response, it remains elusive how the positive selection of GC B cells is modulated posttranscriptionally. In this study, we show that methyltransferase like 14 (Mettl14)–mediated methylation of adenosines at the position N^6 of mRNA (N^6-methyladenosine [m6A]) is essential for the GC B cell response in mice. Ablation of Mettl14 in B cells leads to compromised GC B cell proliferation and a defective Ab response. Interestingly, we unravel that Mettl14-mediated m6A regulates the expression of genes critical for positive selection and cell cycle regulation of GC B cells in a Ythdf2-dependent but Myc-independent manner. Furthermore, our study reveals that Mettl14-mediated m6A modification promotes mRNA decay of negative immune regulators, such as Lax1 and Tipe2, to upregulate genes requisite for GC B cell positive selection and proliferation. Thus, our findings suggest that Mettl14-mediated m6A modification plays an essential role in the GC B cell response. ***The Journal of Immunology*****, 2022, 208: 1924–1936.**

Upon engagement by foreign Ags, resting B cells undergo extensive proliferation and differentiate into long-lived Ab-secreting plasma cells (PCs) and memory B cells, providing an individual with lifelong protective humoral immunity (1). Most long-lived PCs and memory B cells are generated in response to protein Ags in germinal centers (GCs), which are temporary microstructures in the peripheral lymphoid organs such as the spleen and lymph nodes (2). GCs comprise two anatomically and functionally distinct zones, that is, the dark zone (DZ) and light zone (LZ) (3). In the DZ, B cells undergo robust proliferation and somatic hypermutation of their Ig V region genes catalyzed by activation-induced cytidine deaminase (AID, encoded by *Aicda*) (4). In the LZ, where positive and negative selection take place, affinity maturation of Ag-specific BCRs occurs through competition for Ags displayed on the surface of follicular dendritic cells and for the help from the limited number of T follicular helper cells (5, 6). Positively selected LZ B cells with relative high affinity undergo preferential proliferation and then return to the DZ whereas negatively selected B cells with low affinity eventually undergo cell death by apoptosis (7). Thus, GC B cells shuttle between the DZ and LZ of the GC, facilitated by their varying CXCR4 and CXCR5 expression, to undergo multiple rounds of proliferation and mutation of their Ig V region genes (8). The positively selected GC B cells, whose BCRs can bind the specific Ags with high affinities, eventually differentiate into long-lived PCs that exit GCs (9).

During the positive selection of GC B cells, signals transduced by the BCR and costimulatory receptors, such as CD40, coordinately induce the expression of transcription factors Myc and AP4, which further activate Uhrf1 to stimulate cell proliferation (5, 10–13). It has been shown that Myc, a master regulator for cell growth and proliferation, is essential for the positive selection of GC B cells (13–15). In addition, mTORC1 is activated in positively selected LZ B cells and supports DZ B cell proliferation (16). Furthermore, Foxo1 regulates the transition of B cells from the LZ to DZ, and the deletion of Foxo1 blocks the formation of DZ B cells (17, 18). Post-transcriptional gene regulation has recently emerged as another vital regulatory level for the positive selection of GC B cells. For example, the RNA-binding protein PTBP1 controls the GC response by

*Department of Biology, School of Life Sciences, Southern University of Science and Technology, Shenzhen, China; †Department of Computer Science and Engineering, College of Engineering, Southern University of Science and Technology, Shenzhen, China; ‡Singapore Immunology Network, Agency for Science, Technology and Research, Singapore; and §Department of Physiology, Yong Loo Lin School of Medicine, National University of Singapore, Singapore

ORCIDs: 0000-0001-9842-9312 (H.H.); 0000-0002-6364-8790 (J.Z.); 0000-0003-3380-258X (S.-J.J.); 0000-0002-2541-3608 (S.X.); 0000-0002-4525-5205 (X.O.).

Received for publication November 9, 2021. Accepted for publication February 7, 2022.

This work was supported by Shenzhen Science and Technology Innovation Commission Grant JCYJ20190809161807432, Guangdong Basic and Applied Basic Research Foundation Grant 2020A1515010262, National Natural Science Foundation of China Grant 32170882, and the Agency for Science, Technology and Research, Singapore.

H.H. and X.O. conceived the study. H.H., X.O., and S.X. designed the research and wrote the paper. H.H. performed most of the experiments and data analysis. G.Z. performed the experiments of Western blot, dot blot, plasmid construction, and others. J.Z. performed bioinformatics analysis. W.C., Y.L., G.-X.R., R.Z., and J.W. performed animal works. S.-J.J. designed the research and provided constructive suggestions.

The sequencing data presented in this article have been submitted to Sequence Read Archive under accession number PRJNA777821.

Address correspondence and reprint requests to Dr. Sheng-Jian Ji and Dr. Xijun Ou, Department of Biology, School of Life Sciences, Southern University of Science and Technology, 1088 Xueyuan Avenue, Shenzhen 518055, China. E-mail addresses: jisj@sustech.edu.cn (S.-J.J.) and ouxj@sustech.edu.cn (X.O.)

The online version of this article contains supplemental material.

Abbreviations used in this article: AID, activation-induced cytidine deaminase; BM, bone marrow; CGG, chicken γ globulin; DN, DEC-OVA–induced negatively selected; DP, DEC-OVA–induced positively selected; DZ, dark zone; FPKM, fragments per kilobase of transcript per million mapped reads; GC, germinal center; GSEA, gene set enrichment analysis; IGF2BP, insulin-like growth factor 2 mRNA-binding protein; KEGG, Kyoto Encyclopedia of Genes and Genomes; KO, knockout; LZ, light zone; m6A, N^6-methyladenosine; m6A-seq, m6A sequencing; MeRIP, methylated RNA immunoprecipitation; MeRIP-seq, MeRIP sequencing; Mettl3, methyltransferase like 3; Mettl14, methyltransferase like 14; NP, (4-hydroxy-3-nitrophenyl) acetyl; PC, plasma cell; qPCR, quantitative PCR; Ribo-seq, ribosome sequencing; RNA-seq, RNA sequencing; RT-qPCR, real-time qPCR; Tipe2, TNF-α–induced protein 8–like 2; UTR, untranslated region; WT, wild-type; Ythdf2, YTH N^6-methyladenosine RNA-binding protein 2.

regulating mRNA alternative splicing of genes associated with positive selection (19). However, the underlying mechanisms for the positive selection regulation at the posttranscriptional level remain largely unknown.

Methylation of adenosines at the position N^6 of the mRNA (N^6-methyladenosine [m6A]) is the most common posttranscriptional modification of mRNA and plays essential functions in mRNA metabolic processes, including alternative splicing, nuclear export, translation, stability, and degradation of mRNA (20). m6A is a dynamically reversible modification that is mediated by "writers" (methylation) and "erasers" (demethylation). The writer of mRNA m6A is a multiprotein complex mainly composed of methyltransferase like 3 (Mettl3), methyltransferase like 14 (Mettl14) and Wilms' tumor 1–associating protein (Wtap) (21). Mettl3 and Mettl14 perform different functions in the writers complex, in which Mettl3 functions as the core catalytic subunit and Mettl14 facilitates substrate RNA binding. Another group of RNA-binding proteins (m6A readers), such as YTH N^6-methyladenosine RNA-binding protein 2 (Ythdf2) (22) and insulin-like growth factor 2 mRNA-binding proteins (IGF2BPs) (23), can recognize m6A continuous sequence (DRACH motif, D = G/A/U, R = G/A, H = A/U/C) to regulate mRNA degradation and stabilization, which in turn affects a variety of biological processes (24, 25).

Since the first report on the function of m6A in T cell homeostasis (26), a rapidly accumulating body of research has demonstrated that m6A is critical for immune cell development and function. For example, m6A can promote the activation of dendritic cells and play essential roles in anti-tumor immunity (27, 28). In addition, m6A regulates TLR signaling and the activation of macrophages and controls the function of regulatory T cells, preventing spontaneous colitis (29, 30). Furthermore, m6A plays a role in promoting tumor suppression in NK cells (31). More recently, m6A was shown to regulate the transition of pro-B to pre-B cells by controlling mRNA decay in a Ythdf2-dependent manner (32). Although m6A has been shown to play an essential role in early B cell development, its functions in B cell activation and GC response are not fully understood.

In this study, we specifically delete Mettl14, an essential component of the m6A writer complex (33), in B cells. We reveal that loss of Mettl14 in B cells impairs GC B cell responses and diminishes BCR and CD40 signaling in GC B cells. We further demonstrate that the Mettl14/m6A/Ythdf2 axis is critical for the positive selection of GC B cells by inhibiting the expression of negative regulators via mRNA decay.

Materials and Methods

Mice and immunization

Mettl14$^{fl/+}$ mice were purchased from Cyagen and self-crossed to generate *Mettl14*$^{fl/fl}$ mice. CD19$^{Cre/+}$ mice were purchased from Shanghai Model Organisms Center. *Aicda*$^{Cre/+}$ mice were purchased from The Jackson Laboratory. *Ythdf2*$^{fl/fl}$ mice were generated as reported previously (34). The mice used for experiments and breeding were aged 6–10 wk. Mice were immunized with 100 μg of (4-hydroxy-3-nitrophenyl) acetyl $(NP)_{30}$-chicken γ globulin (CGG) (Biosearch Technologies) in aluminum (Thermo Fisher Scientific) by i.p. injection. All mice were housed in a clean and Ag-free environment in the Laboratory Animal Center of Southern University of Science and Technology. All animal experimental operations were approved by the Laboratory Animal Welfare and Ethics Committee of the Southern University of Science and Technology.

Cell culture and cell proliferation assay in vitro

Splenic B cells were purified using anti-CD43 beads (Miltenyi Biotec) and LS columns (Miltenyi Biotec) according to the manufacturer's instructions. B cells were seeded at 4×10^6/ml and cultured in RPMI 1640 medium (Life Technologies) supplemented with 10% FBS (Life Technologies) and 1% penicillin/streptomycin (HyClone). For cell stimulation in vitro, the final concentrations of LPS (Sigma-Aldrich), anti-IgM (Jackson ImmunoResearch), and anti-CD40 (BD Biosciences) were 20, 10, and 1 μg/ml, respectively. For the proliferation assay, cells were stained with CFSE (BioLegend) according to the manufacturer's instructions before culture and then analyzed at the indicated time using flow cytometry.

Flow cytometry and cell sorting

Single-cell suspensions were prepared from mouse spleens, and RBCs were lysed in cold RBC lysis buffer (BioLegend, 420301). Cells were then filtered through 70-μm nylon mesh and counted using a cell counter system (Countstar). After that, cells were stained with appropriate Abs as shown in Supplemental Table I for further analysis. For intracellular staining, cells were fixed and permeabilized using the Foxp3/transcription factor staining buffer set (Invitrogen, 00-5523-00) and stained with appropriate Abs against intracellular proteins as shown in Supplemental Table I. Flow cytometry data were analyzed using FlowJo 10.8.0. Hardy fractions from bone marrow (BM; fractions A–F) were gated as follows: FrA, $B220^+CD43^+BP\text{-}1^-CD24^-$; FrB, $B220^+CD43^+BP\text{-}1^-CD24^+$; FrC, $B220^+CD43^+BP\text{-}1^+CD24^+$; FrC′, $B220^+CD43^+BP\text{-}1^+CD24^{hi}$; FrD, $B220^+CD43^-IgM^-IgD^-$; FrE, $B220^+CD43^-IgM^+IgD^-$; FrF, $B220^+CD43^-IgM^+IgD^+$. BM B cell subsets were also gated as follows: pre-pro, $B220^+CD43^+CD19^-CD25^-$; pro, $B220^+CD43^+CD19^+CD25^-$; large-pre, $B220^+CD43^+CD19^+CD25^+$; small-pre, $B220^+CD43^-IgM^-$; immature, $B220^+CD43^-IgM^+$; recirculating B, $B220^{hi}CD43^-$. Splenic B cell subsets were gated as follows: T1B, $B220^+CD93^+IgM^{hi}CD23^-$; T2B, $B220^+CD93^+IgM^{hi}CD23^+$; T3B, $B220^+CD93^+IgM^{lo}CD23^+$; MZB, $B220^+CD93^-CD21^{hi}CD23^-$; FOB, $B220^+CD93^-CD21^{lo}CD23^+$.

For GC B cell sorting, single-cell suspensions were prepared. Cells were stained with anti-GL7 Ab conjugated with biotin and subsequently incubated with streptavidin MicroBeads (Miltenyi Biotec, 130-048-101). After that, $GL\text{-}7^+$ cells were purified using LS columns (Miltenyi Biotec) according to the manufacturer's instructions. Finally, the purified $GL7^+$ cells were stained with appropriate Abs, as shown in Supplemental Table I for flow sorting.

ELISA and ELISPOT assay

Sera were collected on days 7, 14, 21, and 28, respectively, after NP-CGG immunization. NP-specific Ab levels were measured by ELISA as described previously (35). An ELISPOT assay was performed according to a previous report (36). Briefly, MultiScreen filter plates (Millipore) were coated with NP_{20}-BSA (Biosearch Technologies) in PBS overnight at 4°C. After washing, 1 million splenic cells or 3 million BM cells were plated in each well, and then the plate was incubated at 37°C for 2 h. After washing, the plate was incubated with anti-IgG1 Ab conjugated with biotin (SouthernBiotech, 1140-08) for 1 h, followed by streptavidin–alkaline phosphatase (SouthernBiotech, 7100-04) incubation for 0.5 h. Finally, the dots were visualized by adding the substrate (Mabtech, 3650-10).

JH4 intron mutation analysis

Mutation detection in the JH4 region of IgH was performed according to a previous report (17). In brief, genomic DNA was prepared from sorted GC B cells at day 10 after NP-CGG immunization, and JH4 fragments were amplified using JH4 primers (37) (forward, 5′-TGGAGTTTTCTGAGCATTGCAG-3′; reverse, 5′-TCCTAGGAACCAACTTAAGAGT-3′). Subsequently, the fragments were cloned into the MIGR1 vector for Sanger sequencing. The sequencing data were analyzed using SHMTool (http://shmtool.montefiore.org/cgi-bin/p1).

Cell proliferation and apoptosis assays

Mice were i.p. injected with 1 mg of BrdU (Invitrogen) 2.5 h before sacrifice. Cell proliferation was determined by measuring BrdU incorporation using a BrdU detection kit (BD Biosciences). Apoptosis was determined by using a CaspGLOW fluorescein active caspase staining kit (BioVision, K180-100-1) as described previously (38). Briefly, single-cell suspensions were prepared from mouse spleens and were incubated at 37°C with FITC-VAD-FMK (CaspGLOW kit component) for 1 h. Then, the cells were washed according to the manufacturer's instructions, followed by labeling with appropriate Abs for GC B cell staining and flow cytometric analysis.

m6A dot blot

The m6A dot blot was performed according to a previous report (27). Briefly, RNA was extracted from cells with RNAiso Plus (Takara Bio, 9180), and the concentrations were measured with NanoDrop One (Thermo Scientific). RNA samples were diluted to the indicated concentration, heated to denature at 65°C for 5 min, and loaded onto a positively charged nylon membrane (Roche). Membranes were then UV cross-linked, blocked by 5% (v/v) skim milk (BD Biosciences) TBST buffer, and incubated with m6A Ab (Cell Signaling Technology, 1:1000 diluted) overnight at 4°C. After

washing with TBST buffer, membranes were incubated with HRP-conjugated goat anti-rabbit IgG (Proteintech, SA00001-2) for 1 h at room temperature and then visualized by the addition of diaminobenzidine peroxidase substrate (Yeasen Biotechnology, 36302ES01). The membrane was stained with 0.02% methylene blue (Shanghai Macklin Biochemical) in 0.3 M sodium acetate (pH 5.2) for evaluating RNA amount.

RNA extraction and real-time quantitative PCR

Total RNA was extracted from cells using RNAiso Plus (Takara Bio, 9108) and reversely transcribed into cDNA using RT SuperMix (Vazyme Biotech). ChamQ Universal SYBR quantitative PCR (qPCR) master mix (Vazyme Biotech) was used to perform real-time qPCR (RT-qPCR). The primer sequences for qPCR used in this study were as follows: *Myc* forward, 5′-GTGCTGCAT GAGGAGACACC-3′, *Myc* reverse, 5′-GACCTCTTGGCAGGGGTTTG-3′; Tipe2 (TNF-α–induced protein 8–like 2 [Tnfaip8l2]), forward, 5′-GAAA CATCCAAGGCCAGACT-3′, *Tipe2* reverse, 5′-AAGGACTCCATGGTG CTTGC-3′; *Lax1* forward, 5′-GTCACAAGAAGGAACTCAGAGC-3′, *Lax1* reverse, 5′-CCACAGGATAC AGGCAGCTAT-3′; *Actin* forward, 5′-CG TGAAAAGATGACCCAGATCA-3′, *Actin* reverse, 5′-CACAGCCTGGA TGGCTACGT-3′; *Mettl14* forward, 5′-CCGGGAGCGGCAGAAGTTA-3′, *Mettl14* reverse, 5′-CCAATGCTATCCGCACTCTCA-3′; 18S rRNA forward, 5′-CCGGTACAGTGAAACTGCGA-3′, 18S rRNA reverse, 5′-CCG TCGGCATGTATTA GCTCT-3′.

RNA decay assay

B cells prestimulated with anti-IgM/anti-CD40 for 2 d were plated in 24-well plates (NEST Biotechnology) and treated with 5 μM actinomycin D (Sigma-Aldrich, SBR00013). Cells were then collected at different time points and lysed by RNAiso Plus (Takara Bio, 9108) for RNA extraction. RT-qPCR was performed as described in the preceding section. 18S rRNA was used as an internal control, and the data of time $t = 0$ were used for normalization.

Western blot

Whole-cell proteins were extracted using radioimmunoprecipitation assay buffer (Sigma-Aldrich, R0278) with protease inhibitor mixture (Roche, 05892791001). Proteins were loaded and run on SDS-PAGE gels and transferred to polyvinylidene difluoride membranes. Membranes were probed with Abs against β-actin (Proteintech, 20536-1-AP), Mettl14 (Proteintech, 26158-1-AP), c-Myc (Cell Signaling Technology, 13987), Lax1 (Proteintech, 21557-1-AP), and Tipe2 (Proteintech, 15940-1-AP), respectively, and further incubated with goat anti-rabbit IgG-HRP (Proteintech, SA00001-2). Membranes were visualized using Western chemiluminescent HRP substrate (Millipore, WBKLS0100) and an imaging system (Tanon, 5200).

RNA sequencing and data processing

An RNeasy mini kit (Qiagen) was used to extract total RNA. After quantification, total RNA with an RNA integrity number >6.5 was used for poly(A) mRNA isolation and fragmentation. Library preparation and sequencing were carried out by Genewiz following the standard manufacturer's protocol. The library DNAs were quantified by a Qubit 3.0 fluorometer (Invitrogen, Carlsbad, CA) and sequenced on an Illumina HiSeq instrument using a 2 × 150-bp paired-end sequencing (PE150) configuration. Cutadapt 1.9.1 was used to remove adaptors and clean up raw data to get filtered data. Then, clean data were aligned to GRCm38 (Ensembl) using HISAT2 2.0.1 software. Gene expression levels were calculated by HTSeq 0.6.1 and DESeq2 Bioconductor package was used to analyze differential expression.

m6A sequencing and data processing

Poly(A) RNA was enriched from total RNA by Dynabeads oligo$(dT)_{25}$ (Thermo Fisher Scientific, San Diego, CA, 61005) and then fragmented through a magnesium RNA fragmentation module (NEB, e6150). One-tenth of RNA fragments were used as input, and the rest were incubated with m6A-specific Abs (Synaptic Systems, Göttingen, Germany, 202003) for m6A immunoprecipitation. Then, the immunoprecipitation and input RNAs were used to generate a DNA library and sequenced with a 2 × 150-bp paired-end sequencing (PE150) configuration on an Illumina NovaSeq 6000 performed by LC-Bio Technology following the recommended protocol. fastp was used to verify sequencing quality and remove sequencing adaptors as well as low-quality bases. HISAT2 was used to map reads to the reference genome. The R package exomePeak and ChIPseeker were used for m6A peak calling and annotation. Motif discovery of the called motif was performed by HOMER. Expressions (fragments per kilobase of transcript per million mapped reads [FPKM]) of mRNAs from input libraries were calculated using StringTie. R package edgeR was used to compare the expression of input mRNA between different groups.

Ribo sequencing and data processing

Cyclohexanone with a final concentration of 100 μg/ml was added to the cell culture medium to block translation extension, and the cells were lysed after mixing. Ribosome footprints library preparation and sequencing were performed according to a previous report and carried out by Gene Denovo Biotechnology (Guangzhou, China) following protocols of an NEBNext multiple small RNA library prep set for Illumina (catalog nos. E7300S and E7300L). After removing adaptors and low-quality data, reads mapped to the rRNA database were further removed. The remaining reads were used for reference genome alignment through Bowtie2 with no mismatch parameter. RiboTaper software was used to calculate readings within the open reading frame of coding genes and normalize gene expression levels. Differences in translation efficiency genes between groups were analyzed using RiboDiff.

Transcriptomic enrichment analysis

Gene set enrichment analysis (GSEA) and Kyoto Encyclopedia of Genes and Genomes (KEGG) analyses were performed using OmicStudio tools (https://www.omicstudio.cn/tool). Gene Ontology enrichment analysis was performed using Metascape (https://metascape.org) with an express analysis model.

Sequencing data visualization and statistical analysis

The volcano plot, heatmap, Venn diagram, scatter plot, box plot, and bar plot of sequencing data were obtained using OmicStudio tools (https://www.omicstudio.cn/tool). Integrated Genomics Viewer (http://www.igv.org/) was used for the visualization of m6A peaks. Statistical analysis was performed using GraphPad Prism 7, and the significance tests used are indicated in the figure legends.

Data availability

RNA sequencing (RNA-seq), m6A sequencing (m6A-seq), and ribosome sequencing (Ribo-seq) data reported in this study have been deposited in the Sequence Read Archive database (https://www.ncbi.nlm.nih.gov/bioproject/PRJNA777821) with accession number PRJNA777821.

Results

m6A is induced in BCR-stimulated B cells and is essential for Ab response

To investigate whether m6A plays a role in B cell activation, we first examined the m6A modification level in B cells activated in vitro using dot blotting. We found that the m6A level was significantly induced in B cells stimulated with anti-IgM and anti-CD40 Abs, which engage BCR and CD40 pathways, compared with the unstimulated cells (Fig. 1A). Interestingly, B cells stimulated with LPS, which activates TLR4 (39), exhibited a similar m6A level to the control B cells, suggesting that m6A might play important roles for B cells specifically upon BCR and costimulatory CD40 receptor engagement. We next asked whether the m6A modification is altered in GC B cells, which are induced in vivo mainly through the stimulation of BCR and costimulatory receptors. To this end, we performed the dot blotting on FACS-sorted $B220^+GL7^+CD38^-$ GC and $B220^+GL7^-CD38^+$ non-GC B cells from wild-type (WT) mice immunized with T cell–dependent Ag NP-CGG in alum. We observed that the m6A modification level was significantly elevated in the GC B cells compared with the non-GC B cells (Fig. 1B). These results indicate that m6A modification is enhanced in B cells upon engagement of BCR and costimulatory receptors such as CD40.

To explore the physiological role of m6A in B cell activation and the Ab response, we crossed *Mettl14*$^{fl/fl}$ mice with *Aicda*$^{Cre/+}$ mice to generate *Mettl14*$^{fl/fl}$*Aicda*$^{Cre/+}$ mice, in which the loxP-flanked (floxed) *Mettl14* alleles were deleted specifically by AID-Cre induced in the activated B cells (Supplemental Fig. 1A, 1B). We first challenged *Mettl14*$^{fl/fl}$*Aicda*$^{Cre/+}$ and *Mettl14*$^{fl/fl}$ control mice with NP-CGG in alum and measured the NP-specific Ab levels by ELISA at different time points postimmunization. We found that the NP-specific IgM, IgG1, IgG2b, and IgG3 titers were markedly reduced across the various time points examined in the immunized

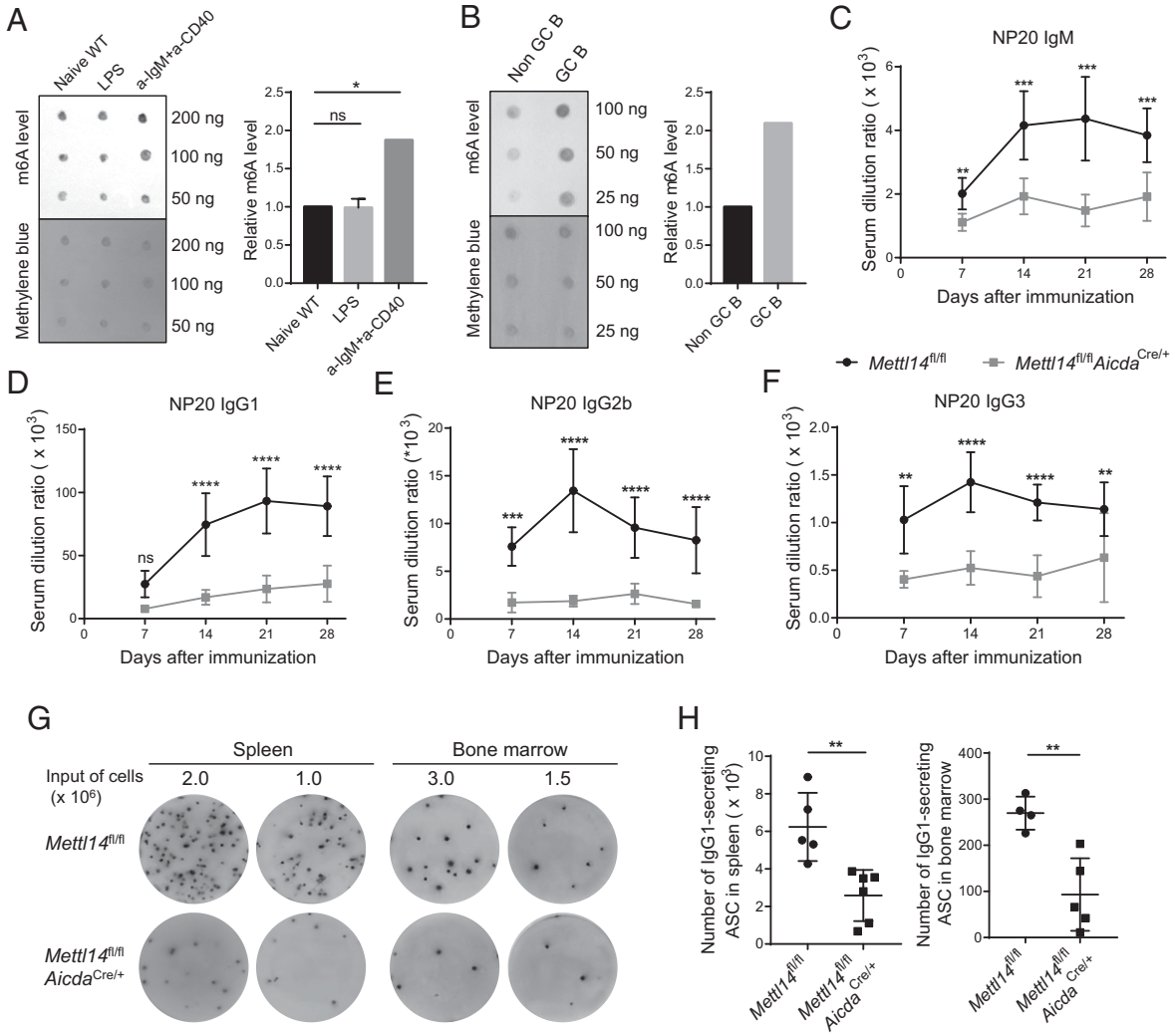

FIGURE 1. m6A is induced in BCR-stimulated B cells and is essential for Ab response. (**A**) m6A dot blot assay of naive B cells and B cells treated with LPS or anti-IgM/anti-CD40 for 2 d. Methylene blue stain was used as a loading control. The amount of RNA is indicated. A two-tailed unpaired Student *t* test was used for statistical analysis. (**B**) m6A dot blot assay of sorted non-GC B cells ($B220^+CD38^+GL7^-$) and GC B cells ($B220^+CD38^-GL7^+$). Methylene blue stain served as a loading control. (**C–F**) ELISA assays to determine the serum Ab titers of NP-specific IgM (C), IgG1(D), IgG2b (E), and IgG3 (F) postimmunization. The serum dilution ratio was calculated as the dilution of serum samples when the OD value reaches 1 ($n = 6–7$; two-way ANOVA). (**G** and **H**) ELISPOT assay (G) and statistical analysis (H) of anti-NP IgG1 Ab-secreting plasma cells in spleen and bone marrow. In (F), each dot represents an individual mouse. Data are from one experiment (C–F), or from one of four independent experiments (G and H). All error bars represent SD. $*p < 0.05$, $**p < 0.01$, $***p < 0.001$, $****p < 0.0001$. ns, not significant ($p > 0.05$).

Mettl14$^{fl/fl}$*Aicda*$^{Cre/+}$ mice than in control mice (Fig. 1C–F). We further assessed the Ab-secreting cells in these mice by ELISPOT assay. It was evident that the frequencies of Ab-secreting cells in the spleen and BM at day 10 postimmunization were significantly reduced in the immunized *Mettl14*$^{fl/fl}$*Aicda*$^{Cre/+}$ mice compared with control mice (Fig. 1G, 1H). These results suggest that Mettl14-mediated m6A modification is vital for the T cell–dependent Ab response.

Mettl14-deficient mice have an impaired GC B cell response

Given the compromised T cell–dependent Ab response in the Mettl14-deficient mice, we moved on to examine whether the GC response is affected in the absence of Mettl14. We assessed the GC B cells 10 d after immunization by flow cytometric analysis using the gating strategy as shown in Supplemental Fig. 1C. We found that the frequency and number of $B220^+Fas^+CD38^-$ GC B cells were reduced by 50% in the spleens of *Mettl14*$^{fl/fl}$*Aicda*$^{Cre/+}$ mice compared with the control mice (Fig. 2A, 2B). Consistently, *Mettl14*$^{fl/fl}$*Aicda*$^{Cre/+}$ mice also exhibited a diminished population of Ag-specific NP^+IgG1^+ B cells in the spleen, as evident by their decreased percentage and absolute number, compared with the control mice (Fig. 2C, 2D). We further dissected the $CXCR4^{hi}CD83^{lo}$ DZ and $CXCR4^{lo}CD83^{hi}$ LZ GC B cells in these mice by flow cytometric analysis. We observed that *Mettl14*$^{fl/fl}$*Aicda*$^{Cre/+}$ mice had a significantly reduced frequency of DZ GC B cells and, therefore, a decreased ratio of DZ to LZ GC B cells (Fig. 2E, 2F). These results suggest that the Mettl14 deficiency causes a diminished GC B cell population and imbalanced DZ and LZ B cell distribution in the GC.

Because the GC response is essential for Ab affinity maturation through somatic hypermutation and positive selection of the Ag-specific B cells, we next evaluated whether the somatic hypermutation is affected by Mettl14 deletion. We extracted DNA from the sorted GC B cells from *Mettl14*$^{fl/fl}$ and *Mettl14*$^{fl/fl}$*Aicda*$^{Cre/+}$ mice and performed Sanger sequencing of the JH4 intron region of the IgH gene. The selection of the JH4 intron region can exclude the effect of affinity selection on somatic mutations (10). The proportion of mutant sequences and the average number of mutations per sequence showed

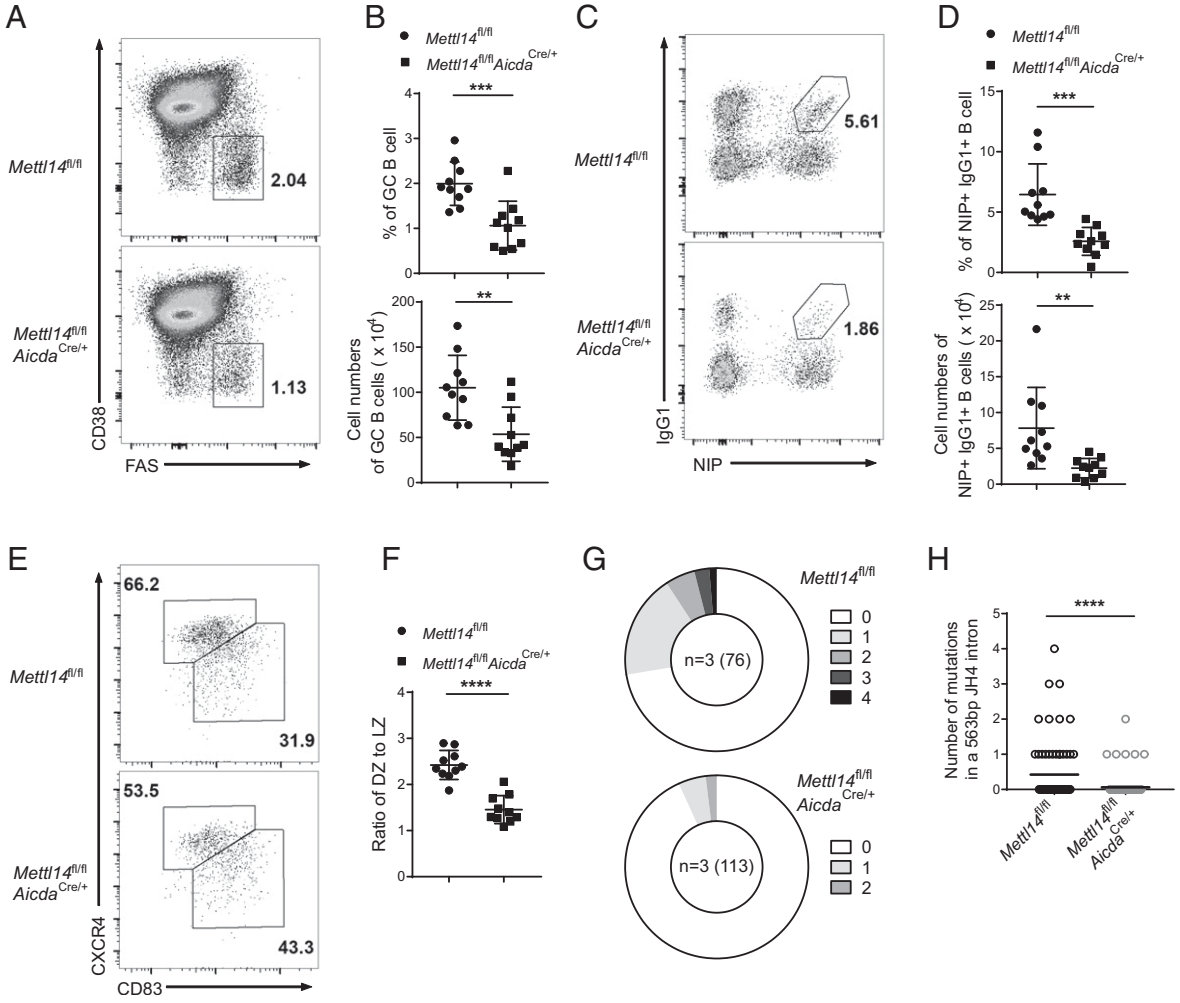

FIGURE 2. Mettl14-deficient mice have an impaired GC B cell response. (**A**) Flow cytometric analysis of GC B cells ($B220^+CD38^-Fas^+$) at day 10 postimmunization. (**B**) Frequencies and numbers of GC B cells as shown in (A). (**C**) Flow cytometric analysis of NP-specific $IgG1^+$ splenic B cells ($B220^+Dump^-NIP^+IgG1^+$) at day 10 postimmunization. (**D**) The frequencies and numbers of NP-specific $IgG1^+$ B cells as shown in (C). (**E**) Flow cytometric analysis of DZ ($B220^+CD38^-Fas^+CD83^{lo}CXCR4^{hi}$) and LZ ($B220^+CD38^-Fas^+CD83^{hi}CXCR4^{lo}$) GC B cells at day 10 postimmunization. (**F**) The ratio of DZ to LZ B cells as shown in (E). In (B), (D), and (F), each symbol represents an individual mouse, and a two-tailed unpaired Student *t* test was used for statistical analysis. (**G**) Pie charts depict the proportions of sequences that carry one, two, three, and four mutations in JH4 intron in GC B cells isolated from three mice of each genotype. The numbers of analyzed sequences are given in the middle of the pie charts. (**H**) Statistical analysis of mutation frequencies in JH4 intron as shown in (G). The black line represents the average of mutation numbers. Data are from one representative of eight independent experiments (A–F), or from one independent experiment (G and H). All error bars represent SD. A Mann–Whitney *U* test was used for statistical analysis in (H). $^{**}p < 0.01$, $^{***}p < 0.001$, $^{****}p < 0.0001$.

that Mettl14-deficient GC B cells exhibited a much lower mutation frequency than did their WT counterparts (Fig. 2G, 2H). Therefore, our results indicate that Mettl14-mediated m6A modification is essential for the GC B cell response.

Mettl14 is indispensable for B cell proliferation upon BCR and CD40 engagement

The decreased GC B cell population in the *Mettl14*$^{fl/fl}$*Aicda*$^{Cre/+}$ mice could result from augmented cell death, impaired cell proliferation, or both in the absence of Mettl14. Thus, we first investigated whether the cell death of the mutant GC B cells is affected by examining the caspase activation in these cells. Flow cytometric analysis revealed that the Mettl14-deficient and control mice had comparable $CaspGLOW^+$ GC B cell populations in the spleens upon immunization with NP-CGG, indicating that the apoptosis of GC B cells was indistinguishable between these mice (Fig. 3A). Next, we investigated the GC B cell proliferation in the immunized mice by performing a BrdU incorporation assay. We observed that *Mettl14*$^{fl/fl}$*Aicda*$^{Cre/+}$ mice had a milder, but statistically significant, decrease in the percentage of $BrdU^+$ GC B cells compared with the control mice (Fig. 3B). Interestingly, we found a substantially reduced BrdU incorporation in the LZ but not DZ GC B cells in *Mettl14*$^{fl/fl}$*Aicda*$^{Cre/+}$ mice (Fig. 3C), indicating a proliferation defect of LZ B cells in the *Mettl14*$^{fl/fl}$*Aicda*$^{Cre/+}$ mice.

GC B cells in the LZ compete for specific Ags displayed by follicular dendritic cells with the help of the T follicular helper cells in a BCR- and CD40-dependent manner (5, 9). Then, the positively selected LZ cells re-enter the cell cycle and travel back to the DZ for further expansion (12). Given that the defective proliferation was evident specifically in the LZ but not DZ B cells of the *Mettl14*$^{fl/fl}$*Aicda*$^{Cre/+}$ mice, we hypothesized that the Mettl14-deficient LZ B cells might have a compromised response to the positive selection signals. To test this possibility, we first analyzed the activation of control and Mettl14-deficient B cells triggered by BCR stimulation in vitro. To this end, we employed naive splenic B cells from the control and *Mettl14*$^{fl/fl}$*Cd19*$^{Cre/+}$ mice, in which the floxed *Mettl14*

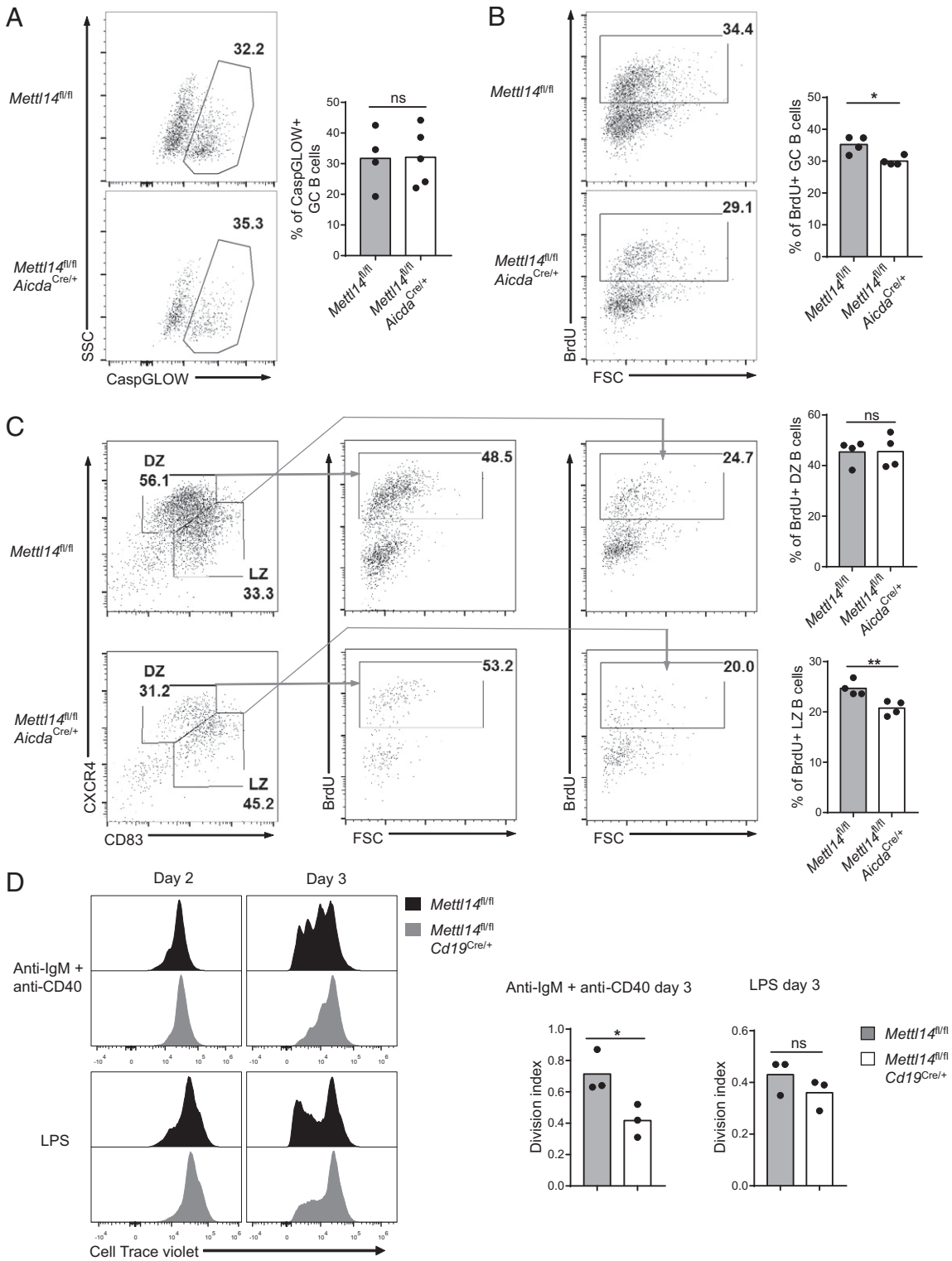

FIGURE 3. Mettl14 is indispensable for B cell proliferation upon BCR and CD40 engagement. (**A**) Flow cytometric analysis of GC B cell apoptosis as detected by caspase activation. (**B**) Flow cytometric analysis GC B cell proliferation as determined by BrdU incorporation. (**C**) Flow cytometric analysis of proliferating DZ and LZ B cells detected by BrdU incorporation. Mice were immunized with NP-CGG and sacrificed for GC response analysis at day 10 (A–C). (**D**) Purified naive B cells were labeled with CFSE and treated with anti-IgM/anti-CD40 and LPS, respectively. B cell proliferation was analyzed at days 2 and 3 postactivation by flow cytometry. Division indexes were calculated using the proliferation modeling analysis of FlowJo software. Each symbol in the statistical graphs represents an individual mouse. All data are pooled from three independent experiments. A two-tailed unpaired Student *t* test was used for statistical analysis. $*p < 0.05$, $**p < 0.01$; ns, not significant ($p > 0.05$).

alleles were ablated in the B cell lineage from the pro-B cell stage onward by the CD19-Cre. Analysis of the *Mettl14*$^{fl/fl}$*Cd19*$^{Cre/+}$ mice showed largely intact B cell development (Supplemental Fig. 2A, 2B). We then stimulated the CFSE-labeled Mettl14-deficient B cells with anti-IgM and anti-CD40 Abs for 3 d and assessed their proliferation. We detected a severely decreased cell

proliferation in the Mettl14-deficient B cells compared with the control B cells, suggesting that Mettl14 is indispensable for BCR- and CD40-induced B cell proliferation. Interestingly, the Mettl14-deficient B cells only displayed a slight decrease in cell proliferation when stimulated with LPS (Fig. 3D), consistent with the largely unaltered m6A modification in LPS-stimulated B cells (Fig. 1A). These results indicate that Mettl14 is crucial for B cell proliferation when the BCR and CD40 are engaged, which mimics the situation where LZ B cells compete for the positive selection signals for their further expansion and differentiation.

Mettl14 modulates the expression of genes involved in cell cycle regulation and positive selection of GC B cells

To explore the underlying mechanisms whereby Mettl14 regulates GC B cell response, we performed RNA-seq analysis on the GC B cells FACS sorted from *Mettl14*$^{fl/fl}$ and *Mettl14*$^{fl/fl}$*Aicda*$^{Cre/+}$ mice. We observed that 52 genes were significantly upregulated whereas 15 genes were downregulated in the mutant GC B cells compared with the control B cells (fold change $\geq$ 1.5; $p \leq 0.05$) (Supplemental Fig. 2C). Furthermore, GSEA uncovered that the cell cycle–related genes, especially those involved in a G_2/M phase transition, were downregulated in the Mettl14-deficient GC B cells (Fig. 4A). These results are consistent with our previous observation that both the proliferation of Mettl14-deficient GC B cells in vivo and B cells stimulated in vitro via the BCR and CD40 pathways were significantly reduced (Fig. 3C, 3D).

We also performed GSEA on genes involved in the positive selection of GC B cells using two previously published gene sets (11, 16). We observed a significant downregulation of the positive selection genes in the Mettl14-deficient GC B cells compared with the control cells (Fig. 4B). Myc has been reported to be highly expressed in the positively selected GC B cells, and the Myc mRNA is also regulated by m6A modifications in other systems (40, 41). These results prompted us to ask whether the Myc expression is affected in the Mettl14-deficient GC B cells. Surprisingly, our RT-qPCR analysis showed comparable Myc mRNA levels in the Mettl14-deficient and control GC B cells (Fig. 4C). Moreover, our flow cytometric analysis detected even slightly increased Myc protein in the mutant GC B cells (Fig. 4D), suggesting that the downregulated genes involved in the cell cycle and positive selection of GC B cells are not due to aberrant Myc expression. In contrast, we detected elevated mRNA and protein levels of Myc in the Mettl14-deficient B cells stimulated in vitro by anti-IgM and anti-CD40 Abs (Fig. 4E, 4F). These results are consistent with the significantly enhanced Myc expression in Mettl14-deficient pro-B cells, as reported previously (32), indicating that Mettl14 might negatively regulate Myc expression. Nevertheless, our data suggest that Mettl14 is essential for the upregulation of genes involved in the proliferation and positive selection of GC B cells.

Mettl14-mediated m6A modification negatively regulates mRNA transcript levels in BCR-stimulated B cells

We next attempted to understand how Mettl14 regulates gene expression in BCR-stimulated B cells. First, we performed m6A dot blotting analysis of the Mettl14-deficient and control B cells stimulated with anti-IgM and anti-CD40 Abs. We detected substantially less abundant m6A modification in the activated Mettl14-deficient B cells than in their control counterparts (Fig. 5A). To obtain a comprehensive view of the global m6A modification network in these cells, we then performed a methylated RNA immunoprecipitation (MeRIP) sequencing (MeRIP-seq, also called m6A-seq) analysis of the activated B cells with and without Mettl14. As it is difficult to obtain enough GC B cells for the MeRIP-seq analysis, we used B cells in vitro stimulated with anti-IgM and anti-CD40 Abs for 2 d as the surrogates of GC B cells undergoing positive selection in vivo, given that our aforementioned data have demonstrated that Mettl14-deficient GC B cells and the mutant B cells stimulated with anti-IgM and anti-CD40 Abs in vitro manifest similar proliferation defects (Fig. 3C, 3D) and downregulated cell cycle–related genes (Fig. 4A, Supplemental Fig. 2D).

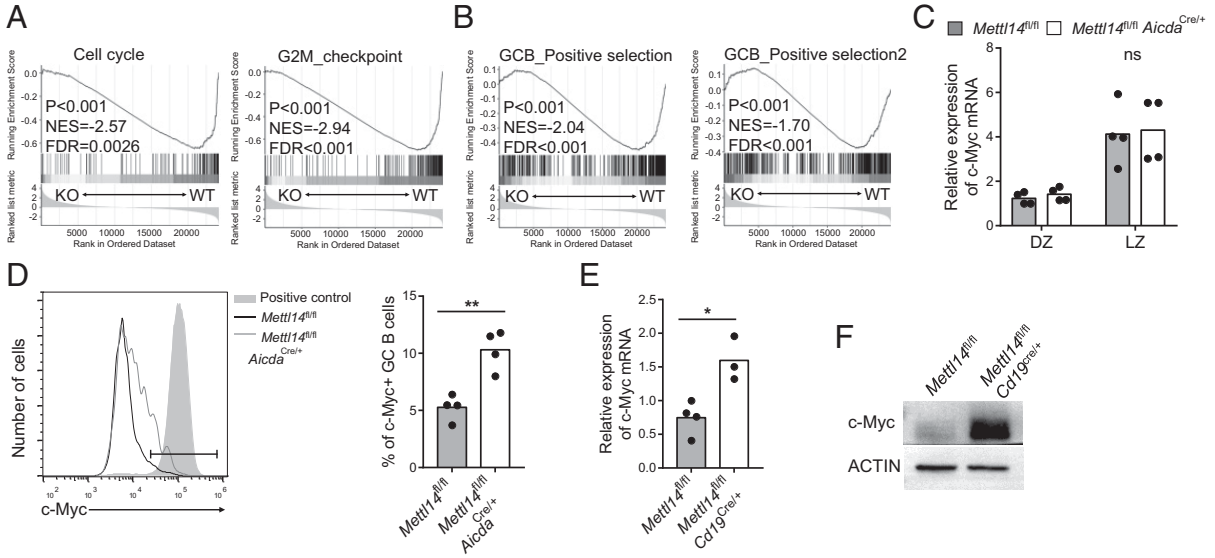

FIGURE 4. Mettl14 modulates the expression of genes involved in cell cycle regulation and positive selection of GC B cells in a Myc-independent manner. (**A** and **B**) GSEA of cell cycle associated-genes (A) and positive selection genes (B) in GC B cells of *Mettl14*$^{fl/fl}$ (WT) and *Mettl14*$^{fl/fl}$*Aicda*$^{Cre/+}$ (KO) mice. For (B), the gene sets were defined as the expression of the top 500 genes that increased significantly ($p \leq 0.05$) in positively selected GC B cells compared with negatively selected GC B cells using published RNA-seq data (GSE98778 and GSE80669). (**C**) The relative expression level of *Myc* mRNA in GC B cells determined by RT-qPCR. (**D**) Flow cytometric analysis of intracellular Myc protein level in GC B cells. B cells from Eu-Myc mice were used as a positive control for gating Myc$^+$ cells. Mice were immunized with NP-CGG and sacrificed at day 10 for GC response analysis (A–D). (**E** and **F**) RT-qPCR (E) and Western blot (F) analysis of Myc expression in anti-IgM/anti-CD40 costimulated B cells. Data are from one representative of two (C) or three (D and E) independent experiments. In (C)–(E), each symbol in the statistical graphs represents an individual mouse, and a two-tailed unpaired Student *t* test was used for statistical analysis. *$p < 0.05$, **$p < 0.01$; ns, not significant ($p > 0.05$).

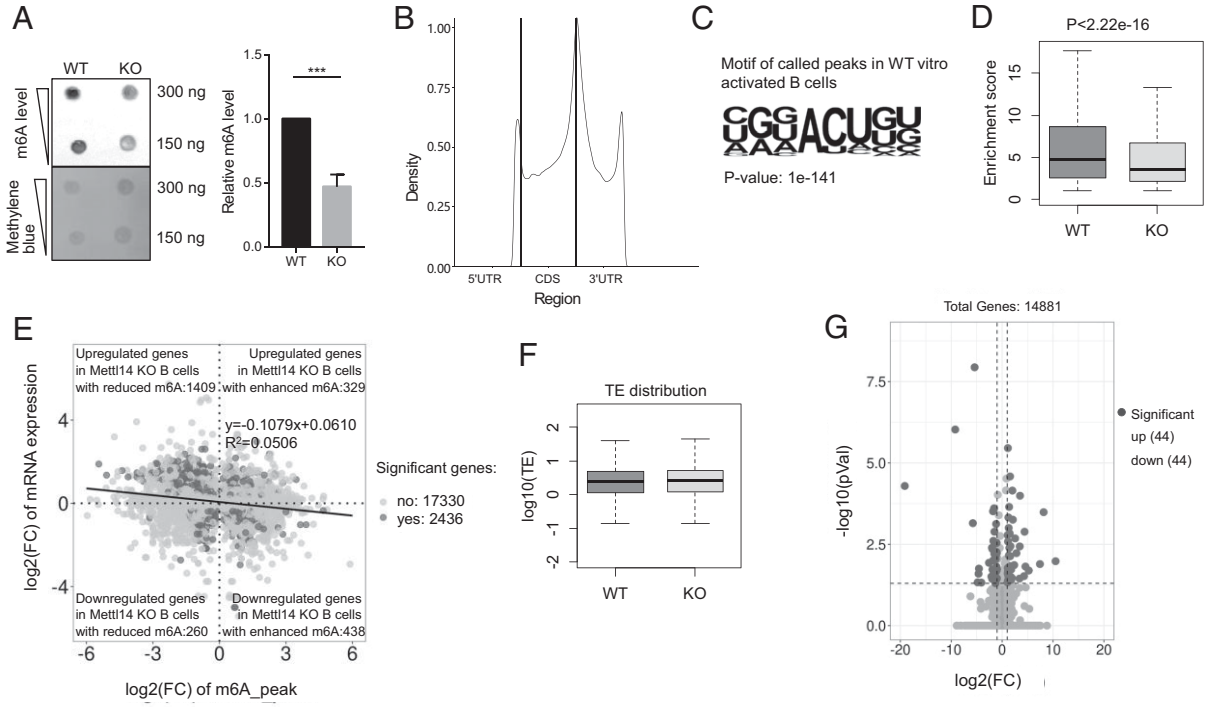

FIGURE 5. Mettl14-mediated m6A modification negatively regulates mRNA transcript levels in BCR-stimulated B cells. (**A**) m6A dot blot assay of anti-IgM/anti-CD40–stimulated B cells of *Mettl14*$^{fl/fl}$ (WT) and *Mettl14*$^{fl/fl}$*Cd19*$^{Cre/+}$ (KO) mice. ***$p < 0.001$. (**B**) Enrichment of WT m6A peaks along with the whole mRNA transcripts. The left vertical line near 5′-UTR indicates the start codon, and the right vertical line near 3′-UTR indicates the stop codon. (**C**) Top enriched sequence motif from the detected WT m6A peaks. (**D**) Box plot showing enrichment scores of called peaks from WT and KO activated B cells. A Mann–Whitney–Wilcoxon test was used for statistical analysis. (**E**) Scatter plot depicting the correlation between mRNA expression and m6A modifications. Significant deferentially expressed genes or m6A modified genes are highlighted in black ($p \leq 0.05$). (**F**) Box plot of gene translation efficiency from WT and KO activated B cells. Translation efficiency is defined as the ratio of translating mRNAs (FPKM in Ribo-seq) to total mRNAs (FPKM in RNA-seq) of a gene. (**G**) Volcano blot of Ribo-seq data from WT and KO activated B cells. Genes with significant differences (fold change ≥ 1.5; $p \leq 0.05$) in translation efficiency are indicated. Activated B cells were in vitro–stimulated B cells with anti-IgM/anti-CD40 Abs for 2 d.

Our MeRIP-seq analysis showed that the overall m6A modification was more enriched in the 3′-untranslated regions (UTRs) proximal to the stop codon than the mRNA coding sequence, the 5′-UTR, and the distal 3′-UTR regions in the activated WT B cells (Fig. 5B). Motif analysis further corroborated that the canonical m6A sequence GGACU is enriched in the m6A peak regions (Fig. 5C), consistent with the previous reports (42–44). Importantly, we found that the overall enrichment score of the m6A modification was significantly lower in the mutant cells than in WT B cells (Fig. 5D). These results indicate that the global m6A modification is markedly disturbed in the activated Mettl14-deficient B cells.

We further investigated the relationship between m6A modification and global gene expression by corresponding m6A sites to genes differentially expressed in the Mettl14-deficient B cells. We found that 1669 differentially expressed genes had reduced m6A modification, whereas 767 genes had enhanced m6A levels. Furthermore, among the 1669 genes with reduced m6A modification in the mutant B cells, 84% (1409) of genes had increased transcript levels, whereas only 16% (260) of the genes displayed decreased transcript levels (Fig. 5E). These results suggest that the m6A modification was negatively correlated with the mRNA transcript levels, consistent with the previous reports showing that m6A modification could modulate mRNA transcript levels primarily by promoting mRNA degradation (22).

The m6A modification is also known to regulate mRNA translation in other immune cells (27, 45). Thus, we also assessed the mRNA translation efficiency in the activated B cells using ribosome profiling (Ribo-seq) analysis. We observed that the overall translational efficiency was comparable between WT and Mettl14-deficient B cells, except for 44 genes having either upregulated or downregulated translational efficiency (Fig. 5F, 5G). These results suggest that Mettl14-mediated m6A has little effect on mRNA translation, consistent with an unaffected mRNA translation efficiency in Mettl14-deficient large pre-B cells as previously reported (32). Therefore, our data suggest that Mettl14 negatively regulates the mRNA transcript levels in an m6A-dependent manner in activated B cells.

Mettl14 regulates the positive selection of GC B cells through Ythdf2-dependent mRNA degradation

m6A-modified mRNAs are known to be regulated by different mechanisms. For example, Ythdf2, an m6A reader, can recognize m6A sites and promote mRNA degradation (46). In contrast, RNA-binding proteins IGF2BPs can stabilize mRNAs by binding m6A-modified mRNAs (23). To further understand how Mettl14-mediated m6A modification regulates mRNA transcript levels, we analyzed our RNA-seq results of the in vitro–stimulated B cells and in vivo GC B cells in detail. The GSEA results showed that genes involved in RNA-degradation pathways were less enriched in the Mettle14-deficient cells, both in in vivo GC B cells and in in vitro–stimulated B cells (Fig. 6A). We also re-examined a set of previously published data on genes involved in the positively and negatively selected GC B cells by focusing genes in RNA-degradation pathways (16). Interestingly, the genes involved in RNA-degradation pathways were more enriched in the positively selected GC B cells than cells undergoing negative selection (Fig. 6B). Taken

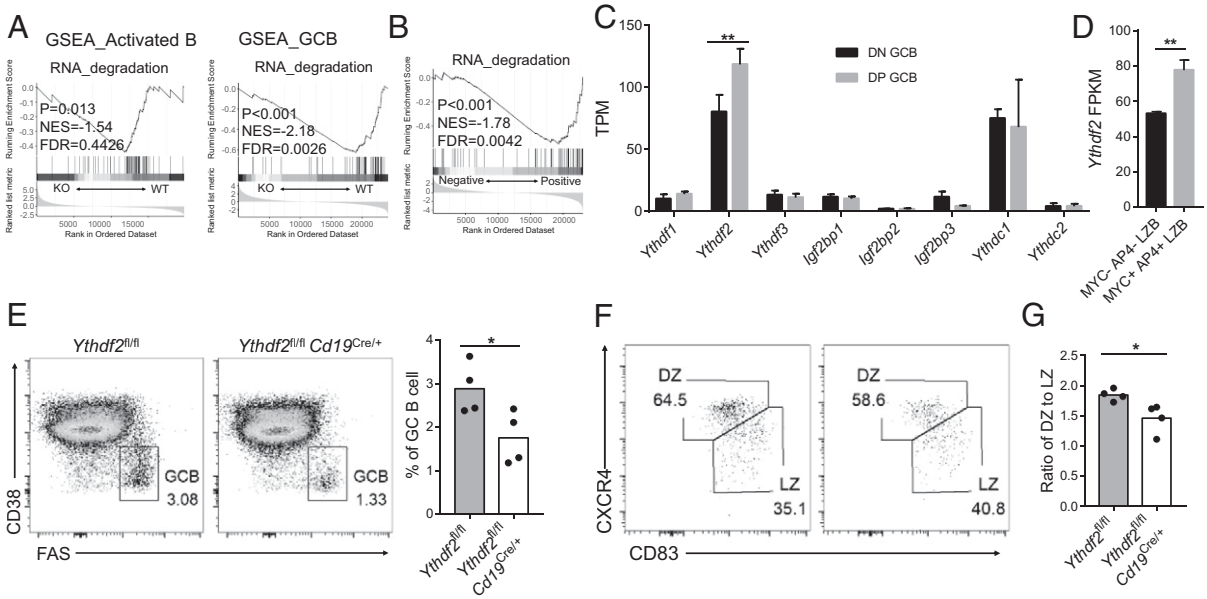

FIGURE 6. Mettl14 regulates the positive selection of GC B cells through Ythdf2-dependent mRNA degradation. (**A** and **B**) GSEA results of RNA degradation were deferentially enriched in anti-IgM/anti-CD40–stimulated B cells and GC B cells after Mettl14 deletion (A) and in positively selected GC B cells (GSE98778, B), respectively. (**C**) Data from GSE98778 showing expression changes of m6A readers in DEC-OVA–induced positively selected (DP) and negatively selected (DN) GC B cells. (**D**) Ythdf2 expression in Myc^+AP4^+ and Myc^-AP4^- LZ B cells from GSE80669. (**E**) Flow cytometric analysis of WT and Ythdf2-deficient GC B cells at day 10 postimmunization. (**F**) Flow cytometric analysis of DZ and LZ B cells as shown in (E). (**G**) Statistical analysis of the ratio of DZ to LZ B cells as shown in (F). Each symbol in statistical graphs represents an individual mouse. Data are pooled from three independent experiments (E–G). A two-tailed unpaired Student *t* test was used for statistical analysis. $*p < 0.05$, $**p < 0.01$.

together, these results suggest that Mettl14-mediated m6A modifications might positively regulate genes involved in mRNA degradation in GC B cells to promote their positive selection.

As Ythdf2 is known to promote mRNA degradation and is required for the transition of pro-B cells to large-pre-B cells (32), we next asked whether Mettl14 regulates the positive selection of GC B cells through Ythdf2-dependent mRNA degradation. Therefore, we re-examined a set of previously published data of the positively selected GC B cells (16) and found that Ythdf2 had the highest expression level among various m6A readers, and the Ythdf2 expression was significantly increased in the positively selected (DEC-OVA–induced positively selected [DP]) GC B cells than their negatively selected (DEC-OVA–induced negatively selected [DN]) counterparts (Fig. 6C). Again, when the data from another separate report (11) were analyzed, we found that the Ythdf2 expression was also higher in the positively selected (Myc^+AP4^+) GC B cells than in the negatively selected (Myc^-AP4^-) GC B cells (Fig. 6D). Taken together, these data imply that Ythdf2 could play an essential role in the positive selection of GC B cells.

To explicitly determine the function of Ythdf2 in GC B cells, we generated $Ythdf2^{fl/fl}CD19^{Cre/+}$ mice, in which Ythdf2 was specifically ablated in B cells. Flow cytometric analysis revealed that $Ythdf2^{fl/fl}CD19^{Cre/+}$ and $Ythdf2^{fl/fl}$ mice had comparable percentages and numbers of various B cell subsets in their BM and spleen (Supplemental Fig. 3A, 3B), suggesting that Ythdf2 is dispensable for B cell development. The unaltered B cell development in $Ythdf2^{fl/fl}CD19^{Cre/+}$ mice made this mouse strain an ideal model for interrogating Ythdf2's role in the GC B cell response. Next, we challenged the $Ythdf2^{fl/fl}CD19^{Cre/+}$ mice with T cell–dependent Ag NP-CGG. We found that the mutant mice exhibited a significantly decreased percentage of GC B cells in their spleens compared with the $Ythdf2^{fl/fl}$ control mice at day 10 postimmunization (Fig. 6E). Intriguingly, we observed that Ythdf2-deficient mice had a diminished DZ GC B cell population and a reduced DZ to LZ B cell ratio (Fig. 6F, 6G), which is almost the same as the phenotype detected in the Mettl14-deficient mice (Fig. 2E, 2F). These results suggest that Ythdf2-dependent mRNA degradation is responsible for the Mettl14--mediated GC B cell positive selection regulation.

Mettl14-mediated m6A downregulates genes for negative immune regulators

So far, our data suggest that Mettl14-mediated m6A modification primarily downregulates mRNA levels through promoting mRNA degradation in the B cells activated via BCR and CD40 stimulation, and the Mettl14 deficiency causes the defective proliferation and positive selection of GC B cells. Thus, we reason that this process could favorably downmodulate genes encoding the negative regulators in these activated B cells. To test this hypothesis, we performed a GSEA of the GC B cells. Interestingly, we found that genes encoding proteins negatively modulating the MAPK signaling cascade and NF-κB transcription factor activity were upregulated in the absence of Mettl14 (Fig. 7A). In addition, KEGG enrichment analysis of downregulated genes in the in vitro–stimulated Mettl14-deficient B cells also picked up MAPK and NF-κB pathways (Fig. 7B). These results suggest that Mettl14-mediated m6A favorably downregulates some signaling molecules playing negative roles in the MAPK and NF-κB pathways and essential for the GC B cell response.

We further interrogated the relationship between m6A modification and gene expression in the activated B cells by overlapping the genes with decreased m6A methylations ($p \leq 0.05$, fold change ≥ 2) and the ones with elevated mRNA levels ($p \leq 0.05$, fold change ≥ 1.5). We obtained a total of 421 such genes, which had reduced m6A modification and increased levels of mRNAs (Fig. 7C). We also determined the overlapping genes that had both decreased m6A modifications and reduced mRNA levels. However, we identified only 16 such genes, and none of them was a cell cycle regulatory gene (Fig. 7C). To further explore the correlation of m6A levels and mRNA level changes, we performed a Fisher exact test using R package GeneOverlap. We found that the genes with decreased m6A

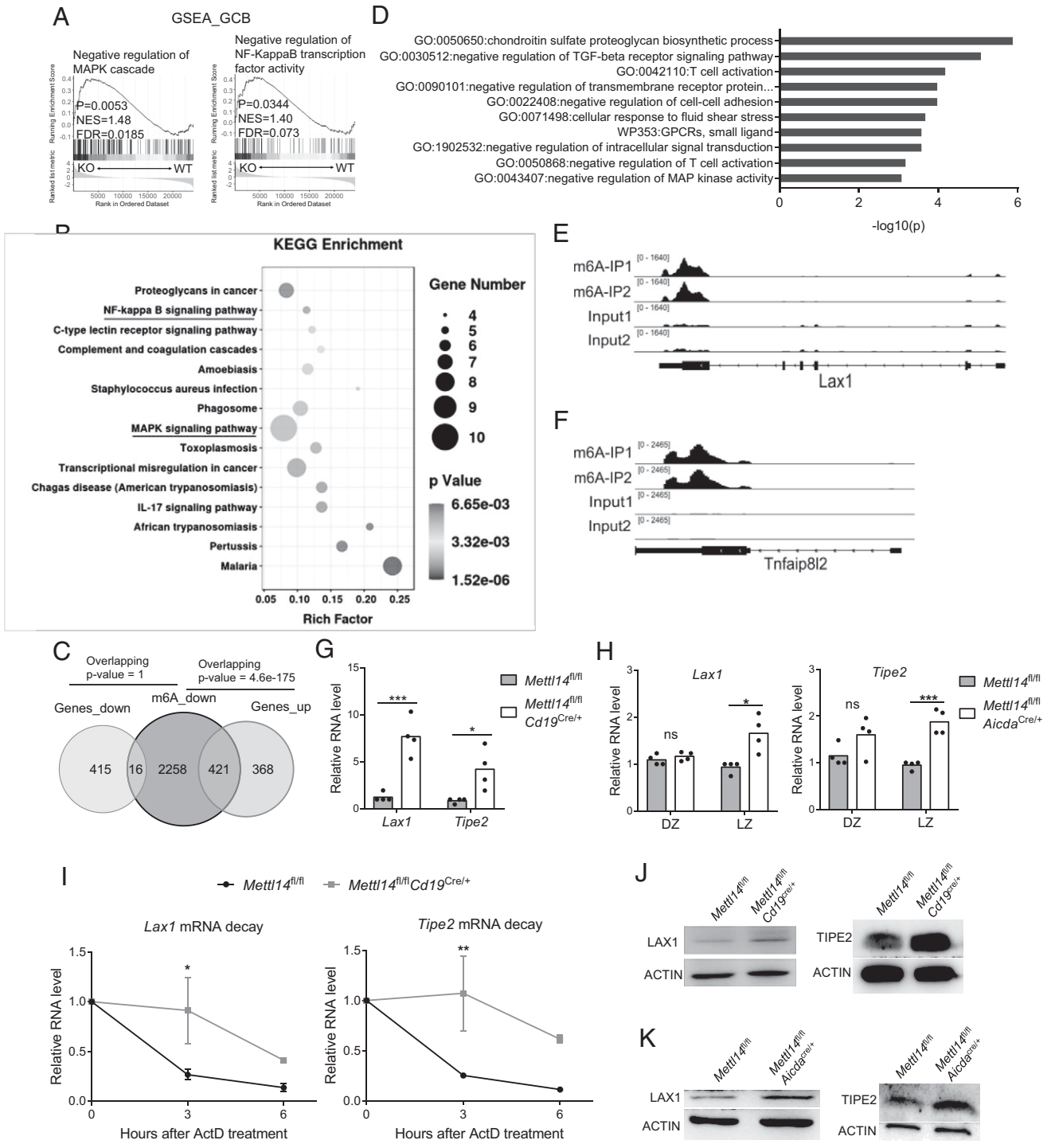

FIGURE 7. Mettl14-mediated m6A downregulates genes for negative immune regulators. (**A** and **B**) GSEA (A) and KEGG enrichment analysis (B) showing that negative regulation of MAPK and NF-κB pathways were differentially enriched in Mettl14-deficient B cells stimulated with anti-IgM/anti-CD40 in vitro for 2 d. (**C**) Pie chart showing the numbers of overlapping and non-overlapping genes between decreased m6A modified genes from m6A-seq data and differentially upregulated or downregulated genes from RNA-seq. (**D**) Gene Ontology enrichment analysis of overlapped genes as shown in (C). (**E** and **F**) Integrated Genomic Viewer views showing m6A methylation sites of Lax1 (E) and Tnfaip8l2 (also named Tipe2, F) of WT B cells stimulated with anti-IgM/anti-CD40 for 2 d. (**G**) RT-qPCR results showing relative expression of Lax1 and Tipe2 in WT and Mettl14-deficient B cells stimulated with anti-IgM/anti-CD40 for 2 d. (**H**) RT-qPCR results of relative expression of *Lax1* and *Tipe2* in WT and Mettl14-deficient DZ and LZ B cells at day 10 postimmunization. (**I**) RNA stability assay of Lax1 and Tipe2 mRNA in WT and Mettl14-deficient B cells stimulated with anti-IgM/anti-CD40 for 2 d. Two-way ANOVA was used for statistical analysis. (**J**) Western blot results showing Lax1 and Tipe2 expression in WT and Mettl14-deficient B cells stimulated with anti-IgM/anti-CD40 for 2 d. (**K**) Western blot results showing Lax1 and Tipe2 expression in WT and Mettl14-deficient GC B cells at day 10 postimmunization. Each symbol in statistical graphs represents an individual mouse. Data are from one representative of two or three independent experiments. A two-tailed unpaired Student *t* test was used for statistical analysis. $*p < 0.05$, $**p < 0.01$, $***p < 0.001$; ns, not significant ($p > 0.05$).

modification were significantly overlapped with the ones with elevated mRNA levels but not the ones with reduced mRNA levels, suggesting that Mettl14-dependent m6A modification mainly downregulates mRNA expression levels. Furthermore, Gene Ontology enrichment analysis of 421 aforementioned overlapping genes unraveled an enrichment of genes involved in several negative

signaling pathways, including the TGF-β receptor signaling pathway, negative regulation of the MAPK pathway, and negative regulation of transmembrane receptor proteins, among others (Fig. 7D). Surprisingly, we did not detect any pathway that is negatively involved in the cell cycle regulation. These results indicate that the Mettl14 deficiency might not immediately result in the upregulation of negative cell cycle regulators, but rather it is directly responsible for the upregulation of genes involved in some negative signaling pathways, which could subsequently affect cell cycle–related genes.

To identify the target genes directly regulated by Mettl14-mediated m6A in GC B cells, we next reanalyzed the previously published RNA-seq data (16). We found that the positively selected (DP) GC B cells had significantly decreased gene expression for a group of negative regulators, such as Lax1, Tipe2 (encoded by *Tnfaip8l2*), and Hivep3, compared with the negatively selected (DN) GC B cells (Supplemental Fig. 3C). Lax1 is an adaptor protein that negatively regulates the activation of immune cells. Previous studies showed that Lax1-deficient mice spontaneously formed GCs, and signaling pathways downstream of the BCR, such as the MAPK pathway, were hyperactivated in the BCR-stimulated Lax1-deficient B cells (47). Furthermore, Tipe2 is another negative immune regulator critical for immune homeostasis, and Tipe2 deficiency causes a spontaneous inflammatory response and hyperactivated MAPK and NF-κB signaling in mice (48). Interestingly, when we further analyzed a set of RNA-seq data from another previously published report (11), we observed that the expression of these genes was similarly dampened in the $Myc^{+}AP4^{+}$ GC B cells (Supplemental Fig. 3D). These results suggest that the Mettl14-mediated m6A modification could directly downmodulate the expression of genes encoding negative regulators, such as Lax1, Tipe2, and Hivep3, in the positively selected GC B cells.

To substantiate whether m6A modification could directly regulate the expression of Lax1 and Tipe2 in activated B cells, we first analyzed called peaks of m6A in our MeRIP-seq data and found that the 3′-UTR regions of *Lax1* and *Tipe2* mRNAs were rich in m6A modifications (Fig. 7E, 7F). The *Lax1* and *Tipe2* transcript levels were consistently elevated in the in vitro–stimulated B cells and the in vivo LZ B cells in the absence of Mettl14, as compared with their Mettl14-sufficient counterparts (Fig. 7G, 7H). To examine whether increased gene expression was due to loss of m6A-mediated RNA degradation, we measured the mRNA life time of Lax1 and Tipe2 by inhibition of transcription with actinomycin D in activated WT and Mettl14-deficient B cells. After treatment with actinomycin D, the Lax1 and Tipe2 mRNAs in Mettl14-deficient cells exhibited greater stability than that in WT cells (Fig. 7I). To further corroborate the upregulation of these negative regulators, we performed immunoblotting to examine their protein levels in the in vitro–activated B cells and the in vivo GC B cells. Compared to the WT cells, Mettl14-deficient GC B cells exhibited much higher Lax1 and Tipe2 protein levels (Fig. 7J, 7K). Taken together, our results suggest that Mettl14-mediated m6A directly targets negative regulator genes *Lax1* and *Tipe2*, and the upregulation of Lax1 and Tipe2 might account for the defective GC B cell response in the mutant mice.

Discussion

In the present study, we investigated the role of Mettl14 in GC B cell responses by using a combination of genetics and transcriptomics approaches. We found that Mettl14-mediated m6A modification positively regulates GC B cell response in a Ythdf2-dependent manner. Mechanistically, our study showed that Mettl14-mediated m6A indirectly upregulates the expression of genes critical for GC B cell positive selection and proliferation by promoting mRNA decay of the genes encoding for a group of negative immune regulators, including Lax1 and Tipe2.

Interestingly, a recent study showed that Mettl3, another essential component of the m6A writer complex, regulates GC B cell responses through both Ythdf2-mediated degradation of oxidative phosphorylation-associated genes and IGF2BP3-enhanced stabilization of m6A-decorated Myc transcripts (49). In our study, we showed that the loss of Mettl14 does not cause a reduction of Myc mRNA levels in GC B cells, but rather it leads to increased Myc protein levels in the GC B and in vitro–stimulated B cells. These results are consistent with the enhanced Myc levels in the Mettl14-deficient pro-B cell (32). Indeed, the abundance of Myc mRNA has been found to be regulated by m6A modifications in many other cell types, including leukemia and hematopoietic stem cells (40, 41, 50). However, even within the same cell type, the function of m6A modifications mediated by different m6A writers differs. Thus, the discrepancy in the Myc mRNA levels resulting from Mettl3 and Mettl14 deficiency might be because the functions of Mettl3 and Mettl14 do not fully overlap, with Mettl3 but not Mettl14 having a methyltransferase activity (51, 52).

Positive selection of GC B cells requires the combinatory activation of BCR and CD40, triggering a myriad of downstream signaling cascades (5). BCR signaling mainly activates the PI3K-AKT pathway, whereas CD40 mainly activates the NF-κB pathway, and both BCR and CD40 signals provoke the MAPK pathways (5, 53–55). Defective MAPK activation impairs GC B cell proliferation and differentiation (56). In our study, loss of Mettl14 suppressed MAPK and NF-κB pathway in activated B cells upon BCR and CD40 engagement, implying that m6A may play an essential role in B cell positive selection through regulating MAPK and NF-κB activation. It has been shown that m6A modulates MAPK and NF-κB pathways in many activated immune cells, such as in LPS-stimulated bone marrow–derived macrophages and dendritic cells (27, 28, 57). These results imply that the m6A modification could control immune cell activation primarily through regulating MAPK and NF-κB activation.

Another interesting finding from our current study is that Lax1 and Tipe2 are upregulated in the activated B cells deficient in Mettl14. Lax1 and Tipe2 are known to exert essential functions in regulating immune cell homeostasis. Lax1 is expressed in both T and B cells and, as a member of the transmembrane adaptor proteins, it binds to Grb2 and p85 to inhibit the MAPK and PI3K-AKT pathways upon BCR or TCR engagement (47, 58). Similarly, Tipe2 negatively modulates NF-κB and MAPK activation in TCR and TLR stimulation to prevent premature mouse death caused by excessive inflammation in mice (48). GC B cells undergoing extensive proliferation need to be tightly controlled, and aberrant activation signaling or transcription factor expression can lead to abnormal GC B cell response and lymphoma (59–61). Previous studies have revealed that GC B cells receiving stronger positive selection signals enter into the cell cycle rapidly, whereas the negatively selected GC B cells are subjected to inefficient cell proliferation and augmented cell death (2, 12). However, the underlying mechanisms for these physiological processes remain unknown. Our findings that the mRNA expression levels of Lax1 and Tipe2 and other immune negative regulators are lower in the positively selected GC B cells than in their negatively selected counterparts imply that these negative regulators exert essential roles during GC B cell selection. Consistently, Lax1-deficient mice displayed more spontaneous GC formation compared with WT mice (47). In our study, the Mettl14-deficient B cells activated via BCR and CD40 engagement manifested an upregulated gene expression for a group of negative immune regulators, including Lax1 and Tipe2 and many others. It is intriguing to speculate that the impaired GC B cell response and

defective positive selection result from a combinatorial effect of the upregulation of a group of negative immune regulators.

In summary, our results demonstrate that the Mettl14-mediated m6A modification decorates the mRNAs of a group of negative immune regulators, such as Lax1 and Tipe2, and promote them to undergo Ythdf2-dependent but Myc-independent degradation, ensuring an effective GC B cell proliferation and positive selection. Therefore, our study uncovers a novel mechanism for GC B cell response regulated by m6A modification.

Acknowledgments

We acknowledge the assistance of SUSTech Core Research Facilities and Laboratory Animal Research Center.

Disclosures

The authors have no financial conflicts of interest.

References

1. Cyster, J. G., and C. D. C. Allen. 2019. B cell responses: cell interaction dynamics and decisions. *Cell* 177: 524–540.
2. Mesin, L., J. Ersching, and G. D. Victora. 2016. Germinal center B cell dynamics. *Immunity* 45: 471–482.
3. Allen, C. D. C., T. Okada, and J. G. Cyster. 2007. Germinal-center organization and cellular dynamics. *Immunity* 27: 190–202.
4. De Silva, N. S., and U. Klein. 2015. Dynamics of B cells in germinal centres. *Nat. Rev. Immunol.* 15: 137–148.
5. Luo, W., F. Weisel, and M. J. Shlomchik. 2018. B cell receptor and CD40 signaling are rewired for synergistic induction of the c-Myc transcription factor in germinal center B cells. *Immunity* 48: 313–326.e5.
6. Lau, A. W. Y., and R. Brink. 2020. Selection in the germinal center. *Curr. Opin. Immunol.* 63: 29–34.
7. Nakagawa, R., A. Toboso-Navasa, M. Schips, G. Young, L. Bhaw-Rosun, M. Llorian-Sopena, P. Chakravarty, A. K. Sesay, G. Kassiotis, M. Meyer-Hermann, and D. P. Calado. 2021. Permissive selection followed by affinity-based proliferation of GC light zone B cells dictates cell fate and ensures clonal breadth. *Proc. Natl. Acad. Sci. USA* 118: e2016425118.
8. Allen, C. D., K. M. Ansel, C. Low, R. Lesley, H. Tamamura, N. Fujii, and J. G. Cyster. 2004. Germinal center dark and light zone organization is mediated by CXCR4 and CXCR5. *Nat. Immunol.* 5: 943–952.
9. Suan, D., C. Sundling, and R. Brink. 2017. Plasma cell and memory B cell differentiation from the germinal center. *Curr. Opin. Immunol.* 45: 97–102.
10. Chen, C., S. Zhai, L. Zhang, J. Chen, X. Long, J. Qin, J. Li, R. Huo, and X. Wang. 2018. Uhrf1 regulates germinal center B cell expansion and affinity maturation to control viral infection. *J. Exp. Med.* 215: 1437–1448.
11. Chou, C., D. J. Verbaro, E. Tonc, M. Holmgren, M. Cella, M. Colonna, D. Bhattacharya, and T. Egawa. 2016. The transcription factor AP4 mediates resolution of chronic viral infection through amplification of germinal center B cell responses. *Immunity* 45: 570–582.
12. Shlomchik, M. J., W. Luo, and F. Weisel. 2019. Linking signaling and selection in the germinal center. *Immunol. Rev.* 288: 49–63.
13. Dominguez-Sola, D., G. D. Victora, C. Y. Ying, R. T. Phan, M. Saito, M. C. Nussenzweig, and R. Dalla-Favera. 2012. The proto-oncogene MYC is required for selection in the germinal center and cyclic reentry. *Nat. Immunol.* 13: 1083–1091.
14. Calado, D. P., Y. Sasaki, S. A. Godinho, A. Pellerin, K. Köchert, B. P. Sleckman, I. M. de Alborán, M. Janz, S. Rodig, and K. Rajewsky. 2012. The cell-cycle regulator c-Myc is essential for the formation and maintenance of germinal centers. *Nat. Immunol.* 13: 1092–1100.
15. Finkin, S., H. Hartweger, T. Y. Oliveira, E. E. Kara, and M. C. Nussenzweig. 2019. Protein Amounts of the MYC transcription factor determine germinal center B cell division capacity. *Immunity* 51: 324–336.e5.
16. Ersching, J., A. Efeyan, L. Mesin, J. T. Jacobsen, G. Pasqual, B. C. Grabiner, D. Dominguez-Sola, D. M. Sabatini, and G. D. Victora. 2017. Germinal center selection and affinity maturation require dynamic regulation of mTORC1 kinase. *Immunity* 46: 1045–1058.e6.
17. Dominguez-Sola, D., J. Kung, A. B. Holmes, V. A. Wells, T. Mo, K. Basso, and R. Dalla-Favera. 2015. The FOXO1 transcription factor instructs the germinal center dark zone program. *Immunity* 43: 1064–1074.
18. Sander, S., V. T. Chu, T. Yasuda, A. Franklin, R. Graf, D. P. Calado, S. Li, K. Imami, M. Selbach, M. Di Virgilio, et al. 2015. PI3 kinase and FOXO1 transcription factor activity differentially control B cells in the germinal center light and dark zones. *Immunity* 43: 1075–1086.
19. Monzón-Casanova, E., M. Screen, M. D. Díaz-Muñoz, R. M. R. Coulson, S. E. Bell, G. Lamers, M. Solimena, C. W. J. Smith, and M. Turner. 2018. The RNA-binding protein PTBP1 is necessary for B cell selection in germinal centers. *Nat. Immunol.* 19: 267–278.
20. Zaccara, S., R. J. Ries, and S. R. Jaffrey. 2019. Reading, writing and erasing mRNA methylation. *Nat. Rev. Mol. Cell Biol.* 20: 608–624.
21. Shi, H., J. Wei, and C. He. 2019. Where, when, and how: context-dependent functions of RNA methylation writers, readers, and erasers. *Mol. Cell* 74: 640–650.
22. Wang, X., Z. Lu, A. Gomez, G. C. Hon, Y. Yue, D. Han, Y. Fu, M. Parisien, Q. Dai, G. Jia, et al. 2014. N^6-methyladenosine-dependent regulation of messenger RNA stability. *Nature* 505: 117–120.
23. Huang, H., H. Weng, W. Sun, X. Qin, H. Shi, H. Wu, B. S. Zhao, A. Mesquita, C. Liu, C. L. Yuan, et al. 2018. Recognition of RNA N^6-methyladenosine by IGF2BP proteins enhances mRNA stability and translation. [Published errata appear in 2018 *Nat. Cell Biol.* 20: 1098 and 2020 *Nat. Cell Biol.* 22: 1288.] *Nat. Cell Biol.* 20: 285–295.
24. Liu, C., Z. Yang, R. Li, Y. Wu, M. Chi, S. Gao, X. Sun, X. Meng, and B. Wang. 2021. Potential roles of N6-methyladenosine (m6A) in immune cells. *J. Transl. Med.* 19: 251.
25. Shulman, Z., and N. Stern-Ginossar. 2020. The RNA modification N^6-methyladenosine as a novel regulator of the immune system. *Nat. Immunol.* 21: 501–512.
26. Li, H.-B., J. Tong, S. Zhu, P. J. Batista, E. E. Duffy, J. Zhao, W. Bailis, G. Cao, L. Kroehling, Y. Chen, et al. 2017. m^6A mRNA methylation controls T cell homeostasis by targeting the IL-7/STAT5/SOCS pathways. *Nature* 548: 338–342.
27. Wang, H., X. Hu, M. Huang, J. Liu, Y. Gu, L. Ma, Q. Zhou, and X. Cao. 2019. Mettl3-mediated mRNA m^6A methylation promotes dendritic cell activation. *Nat. Commun.* 10: 1898.
28. Yin, H., X. Zhang, P. Yang, X. Zhang, Y. Peng, D. Li, Y. Yu, Y. Wu, Y. Wang, J. Zhang, et al. 2021. RNA m6A methylation orchestrates cancer growth and metastasis via macrophage reprogramming. *Nat. Commun.* 12: 1394.
29. Tong, J., X. Wang, Y. Liu, X. Ren, A. Wang, Z. Chen, J. Yao, K. Mao, T. Liu, F.-L. Meng, et al. 2021. Pooled CRISPR screening identifies m^6A as a positive regulator of macrophage activation. *Sci. Adv.* 7: eabd4742.
30. Lu, T. X., Z. Zheng, L. Zhang, H.-L. Sun, M. Bissonnette, H. Huang, and C. He. 2020. A new model of spontaneous colitis in mice induced by deletion of an RNA m^6A methyltransferase component METTL14 in T cells. *Cell. Mol. Gastroenterol. Hepatol.* 10: 747–761.
31. Song, H., J. Song, M. Cheng, M. Zheng, T. Wang, S. Tian, R. A. Flavell, S. Zhu, H.-B. Li, C. Ding, et al. 2021. METTL3-mediated m^6A RNA methylation promotes the anti-tumour immunity of natural killer cells. *Nat. Commun.* 12: 5522.
32. Zheng, Z., L. Zhang, X.-L. Cui, X. Yu, P. J. Hsu, R. Lyu, H. Tan, M. Mandal, M. Zhang, H.-L. Sun, et al. 2020. Control of early B cell development by the RNA N^6-methyladenosine methylation. *Cell Rep.* 31: 107819.
33. Liu, J., Y. Yue, D. Han, X. Wang, Y. Fu, L. Zhang, G. Jia, M. Yu, Z. Lu, X. Deng, et al. 2014. A METTL3-METTL14 complex mediates mammalian nuclear RNA N^6-adenosine methylation. *Nat. Chem. Biol.* 10: 93–95.
34. Yu, J., Y. She, L. Yang, M. Zhuang, P. Han, J. Liu, X. Lin, N. Wang, M. Chen, C. Jiang, et al. 2021. The m6A readers YTHDF1 and YTHDF2 synergistically control cerebellar parallel fiber growth by regulating local translation of the key Wnt5a signaling components in axons. *Adv. Sci.* 8: 2101329.
35. Ou, X., S. Xu, Y. F. Li, and K. P. Lam. 2014. Adaptor protein DOK3 promotes plasma cell differentiation by regulating the expression of programmed cell death 1 ligands. *Proc. Natl. Acad. Sci. USA* 111: 11431–11436.
36. Xu, S., X. Ou, J. Huo, K. Lim, Y. Huang, S. Chee, and K. P. Lam. 2015. Mir-17-92 regulates bone marrow homing of plasma cells and production of immunoglobulin G2c. *Nat. Commun.* 6: 6764.
37. Gitlin, A. D., Z. Shulman, and M. C. Nussenzweig. 2014. Clonal selection in the germinal centre by regulated proliferation and hypermutation. *Nature* 509: 637–640.
38. Xu, S., J. Huo, Y. Huang, M. Aw, S. Chen, S. Mak, L. Y. Yip, Y. S. Ho, S. W. Ng, A. H.-M. Tan, et al. 2019. von Hippel-Lindau protein maintains metabolic balance to regulate the survival of naive B lymphocytes. *iScience* 17: 379–392.
39. Guijarro-Muñoz, I., M. Compte, A. Álvarez-Cienfuegos, L. Álvarez-Vallina, and L. Sanz. 2014. Lipopolysaccharide activates Toll-like receptor 4 (TLR4)-mediated NF-κB signaling pathway and proinflammatory response in human pericytes. *J. Biol. Chem.* 289: 2457–2468.
40. Vu, L. P., B. F. Pickering, Y. Cheng, S. Zaccara, D. Nguyen, G. Minuesa, T. Chou, A. Chow, Y. Saletore, M. MacKay, et al. 2017. The N^6-methyladenosine (m^6A)-forming enzyme METTL3 controls myeloid differentiation of normal hematopoietic and leukemia cells. *Nat. Med.* 23: 1369–1376.
41. Weng, H., H. Huang, H. Wu, X. Qin, B. S. Zhao, L. Dong, H. Shi, J. Skibbe, C. Shen, C. Hu, et al. 2018. METTL14 inhibits hematopoietic stem/progenitor differentiation and promotes leukemogenesis via mRNA m^6A modification. *Cell Stem Cell* 22: 191–205.e9.
42. Meyer, K. D., Y. Saletore, P. Zumbo, O. Elemento, C. E. Mason, and S. R. Jaffrey. 2012. Comprehensive analysis of mRNA methylation reveals enrichment in 3′ UTRs and near stop codons. *Cell* 149: 1635–1646.
43. Garcia-Campos, M. A., S. Edelheit, U. Toth, M. Safra, R. Shachar, S. Viukov, R. Winkler, R. Nir, L. Lasman, A. Brandis, et al. 2019. Deciphering the "m^6A code" via antibody-independent quantitative profiling. *Cell* 178: 731–747.e16.
44. Dominissini, D., S. Moshitch-Moshkovitz, S. Schwartz, M. Salmon-Divon, L. Ungar, S. Osenberg, K. Cesarkas, J. Jacob-Hirsch, N. Amariglio, M. Kupiec, et al. 2012. Topology of the human and mouse m6A RNA methylomes revealed by m6A-seq. *Nature* 485: 201–206.
45. Han, D., J. Liu, C. Chen, L. Dong, Y. Liu, R. Chang, X. Huang, Y. Liu, J. Wang, U. Dougherty, et al. 2019. Anti-tumour immunity controlled through mRNA m^6A methylation and YTHDF1 in dendritic cells. [Published erratum appears in 2019 *Nature* 568: E3.] *Nature* 566: 270–274.
46. Du, H., Y. Zhao, J. He, Y. Zhang, H. Xi, M. Liu, J. Ma, and L. Wu. 2016. YTHDF2 destabilizes m^6A-containing RNA through direct recruitment of the CCR4-NOT deadenylase complex. *Nat. Commun.* 7: 12626.

47. Zhu, M., O. Granillo, R. Wen, K. Yang, X. Dai, D. Wang, and W. Zhang. 2005. Negative regulation of lymphocyte activation by the adaptor protein LAX. *J. Immunol.* 174: 5612–5619.
48. Sun, H., S. Gong, R. J. Carmody, A. Hilliard, L. Li, J. Sun, L. Kong, L. Xu, B. Hilliard, S. Hu, et al. 2008. TIPE2, a negative regulator of innate and adaptive immunity that maintains immune homeostasis. *Cell* 133: 415–426.
49. Grenov, A. C., L. Moss, S. Edelheit, R. Cordiner, D. Schmiedel, A. Biram, J. H. Hanna, T. H. Jensen, S. Schwartz, and Z. Shulman. 2021. The germinal center reaction depends on RNA methylation and divergent functions of specific methyl readers. *J. Exp. Med.* 218: e20210360.
50. Cheng, Y., H. Luo, F. Izzo, B. F. Pickering, D. Nguyen, R. Myers, A. Schurer, S. Gourkanti, J. C. Brüning, L. P. Vu, et al. 2019. m^{6}A RNA methylation maintains hematopoietic stem cell identity and symmetric commitment. *Cell Rep.* 28: 1703–1716.e6.
51. Wang, X., J. Feng, Y. Xue, Z. Guan, D. Zhang, Z. Liu, Z. Gong, Q. Wang, J. Huang, C. Tang, et al. 2016. Structural basis of N^6-adenosine methylation by the METTL3-METTL14 complex. [Published erratum appears in 2017 *Nature* 542: 260.] *Nature* 534: 575–578.
52. Bokar, J. A., M. E. Shambaugh, D. Polayes, A. G. Matera, and F. M. Rottman. 1997. Purification and cDNA cloning of the AdoMet-binding subunit of the human mRNA (N^6-adenosine)-methyltransferase. *RNA* 3: 1233–1247.
53. Khiem, D., J. G. Cyster, J. J. Schwarz, and B. L. Black. 2008. A p38 MAPK-MEF2C pathway regulates B-cell proliferation. *Proc. Natl. Acad. Sci. USA* 105: 17067–17072.
54. Basso, K., U. Klein, H. Niu, G. A. Stolovitzky, Y. Tu, A. Califano, G. Cattoretti, and R. Dalla-Favera. 2004. Tracking CD40 signaling during germinal center development. *Blood* 104: 4088–4096.
55. Batlle, A., V. Papadopoulou, A. R. Gomes, S. Willimott, J. V. Melo, K. Naresh, E. W. F. Lam, and S. D. Wagner. 2009. CD40 and B-cell receptor signalling induce MAPK family members that can either induce or repress Bcl-6 expression. *Mol. Immunol.* 46: 1727–1735.
56. Gallagher, E., T. Enzler, A. Matsuzawa, A. Anzelon-Mills, D. Otero, R. Holzer, E. Janssen, M. Gao, and M. Karin. 2007. Kinase MEKK1 is required for CD40-dependent activation of the kinases Jnk and p38, germinal center formation, B cell proliferation and antibody production. *Nat. Immunol.* 8: 57–63.
57. Wang, X., Y. Ji, P. Feng, R. Liu, G. Li, J. Zheng, Y. Xue, Y. Wei, C. Ji, D. Chen, and J. Li. 2021. The m6A reader IGF2BP2 regulates macrophage phenotypic activation and inflammatory diseases by stabilizing TSC1 and PPARγ. *Adv. Sci. (Weinh.)* 8: 2100209.
58. Zhu, M., I. Rhee, Y. Liu, and W. Zhang. 2006. Negative regulation of FcεRI-mediated signaling and mast cell function by the adaptor protein LAX. *J. Biol. Chem.* 281: 18408–18413.
59. Basso, K. 2021. Biology of germinal center B cells relating to lymphomagenesis. *HemaSphere* 5: e582.
60. Basso, K., and R. Dalla-Favera. 2015. Germinal centres and B cell lymphomagenesis. *Nat. Rev. Immunol.* 15: 172–184.
61. Mintz, M. A., and J. G. Cyster. 2020. T follicular helper cells in germinal center B cell selection and lymphomagenesis. *Immunol. Rev.* 296: 48–61.